Heliyon 9 (2023) e12663

Contents lists available at ScienceDirect

Heliyon

journal homepage: www.cell.com/heliyon

Research article

Structural, electronic and nonlinear optical properties, reactivity and solubility of the drug dihydroartemisinin functionalized on the carbon nanotube

D. Fouejio [a,*], Y. Tadjouteu Assatse [a], R.A. Yossa Kamsi [a], G.W. Ejuh [b,c], J.M.B. Ndjaka [a]

[a] Materials Science Laboratory, Department of Physics, Faculty of Sciences, University of Yaoundé I, P.O. Box 812, Yaoundé, Cameroon
[b] University of Dschang, IUT-FV Bandjoun, Department of General and Scientific Studies, P.O. Box 134, Bandjoun, Cameroon
[c] University of Bamenda, National Higher Polytechnic Institute, Department of Electrical and Electronic Engineering, P. O. Box 39, Bambili, Cameroon

ARTICLE INFO

Keywords:
Dihydroartemisinin
Functionalized CNTs
Targeted drug delivery
Reactivity and solubility
Energy gap
DFT

ABSTRACT

Density functional theory (DFT) calculations of the antimalarial drug dihydroartemisinin (DHA) functionalized on the carbon nanotube (CNT) were carried out in gas phase and in solution to investigate the role of fCNTs as a nanovector for the targeted delivery of the DHA drug and to predict their chemical descriptors and electronic and nonlinear optical (NLO) properties. The results of the geometric optimization indicate that the functionalization does not change the molecular structure of DHA. Based on our findings of binding and solvation energies, two energetically stable configurations were identified in 1st (fCNT1-2) and 2nd (2fCNT1-2) functionalization. For these stable configurations, the energy gap value goes from 1.52 eV for the (5,5) single wall pristine CNT to 1.27 eV for the 1st functionalization and to 1.06 eV for the 2nd functionalization regardless of the considered media; which gives these nanostructures excellent semiconductor properties. Findings from global reactivity descriptors show that the reactivity of the functionalized CNT is strongly improved in solvent media and that the stability of DHA decreases while its reactivity increases during the functionalization. Thus, the fundamental gap (E_f) in gas phase decreases from 3.65 eV for the virgin CNT to 3.30 eV for fCNT2 and to 3.02 eV for 2fCNT2. On the contrary, in water E_f goes from 1.20 eV for the virgin CNT to 0.95 eV for fCNT2 and to 0.74 eV for 2fCNT2; demonstrating an improvement in the reactivity of our fCNTs as nanovectors for targeted delivery of DHA drug. Finally, our findings show that these nanostructures may also have good NLO properties and can be promising materials for NLO applications.

1. Introduction

The discovery in 1991 of carbon nanotubes by Sumio Iijima [1] generated an unprecedented interest in carbon nanostructures, and led several research, both fundamental and applied, in the field of nanotechnologies. They have exceptional physical, chemical and biological properties in many respects and their nanometric size gives them many applications. Due to their exceptional properties,

* Corresponding author.
E-mail address: fouejiodavid@gmail.com (D. Fouejio).

https://doi.org/10.1016/j.heliyon.2022.e12663
Received 6 September 2022; Received in revised form 20 December 2022; Accepted 20 December 2022
Available online 2 January 2023

which result directly from their structural affiliation with graphite, research laboratories and industries have developed CNT synthesis methods including temperature sublimation and condensation under an inert atmosphere of graphite carbon [2], approach based on hemispherical polyarene templates [3] and many other synthesis methods [4,5]. From an electrical and optical point of view, CNTs depending on their geometry, have the particularity of being able to be either metallic or semiconductor with a gap equivalent to that of silicon (1.14 eV) or germanium (0.67 eV) [6]. The semiconductor properties of CNTs are attracting a lot of attention in current research, as they open the way for the development of high-performance field-effect transistors [7-9]. Due to its remarkable optical properties, CNTs are used for the development of optical and optoelectronic devices [10-13]. In addition to their applications in electronics and optics, they are also given therapeutic applications. As fact, they are subject of intense research in the pharmaceutical industry as nanovectors for drug administration and targeted delivery of therapeutic compounds [14,15]. On the other hand, the possibility of functionalizing their surface by appropriate molecular grafting allows them to very easily cross cell walls such as the blood-brain barrier [16], and also to circulate in the body with little of interaction to reach the target organs. However, they have defects such as toxicity and low solubility which limit their application to the biological fields. According to many authors [17], problems related with the efficient administration of drugs, such as limited solubility, poor biodistribution and tissue damage, can be super passed by the use of drug delivery systems. Indeed, due to high drug loading capacities and good cell penetration qualities, surface functionalized CNTs have been proposed as efficient nanovectors for the drug delivery of therapeutic compounds [18-20].

The objective of this work is to functionalize dihydroartemisinin on the carbon nanotube in order to use it as a nanovector for the targeted treatment of malaria. In fact, according to the World Health Organization (WHO), despite all the advances in research, 409,000 deaths from malaria were still recorded worldwide in 2019 [21]. This is partly attributed to the resistance of the malaria parasites to certain drugs. Thus, it is urgent to seek targeted treatments with appropriate administration methods. To date, many theoretical and experimental studies have been carried out on the functionalization of antimalarial molecules on fullerene C_{60} with fairly satisfactory results [22-25].

According to Haynes [26], DHA is a molecule isolated from Artemisia annua leaves. As mentioned above, it is one of drugs used to treat malaria. Moreover, Naderi et al. [27] have recently shown by energetic and structural studies using DFT that the functionalization of DHA on CNT is possible either directly or through the COOH- and COCl-radicals. Both experimental [28] and theoretical [29] studies have shown that the functionalization of azomethine ylide on the surface of CNTs is possible. As fact, Georgakilas et al. [30] experimentally showed that azomethine ylide molecules can easily be functionalized on CNT by 1,3-diploar cycloaddition (DC).

The aim of the present work is by functionalization of DHA on the (5,5) single wall carbon nanotube (SWCNT, $C_{60}H_{20}$) using 1,3-DC reaction of azomethine ylide, to improve the targeted delivery of the DHA drug and model new nanometric compounds for applications in nanotechnologies. In this research work, the stability of the modeled structure through geometrical optimization, binding energy and solvation energy were firstly investigated. Secondly, the electronic and nonlinear optical properties and the global reactivity descriptors of our modeled systems were assessed. Finally, the impact of the functionalization site and the number of functionalization were analyzed.

The remaining part of this paper is organized as follows. In Section 2, we present the methodology used and the computational details. Section 3 contains the presentation and discussion of our findings. Summary and conclusion are given in Section 4.

2. Methodology

DFT method was used in this work to investigate the reactivity, electronic structure properties and NLO properties of the DHA ($C_{15}H_{24}O_5$) covalently bound to (5,5) CNT using 1,3-DC of azomethine ylide (C_2H_5N). The functionalization was done on one site, fCNT, then on two sites, 2fCNT. The calculations were performed in gas phase, then in water and chloroform media using the Gaussian 09D quantum chemical software [31]. The preparation of the calculation files and the visualization of the optimized structures were achieved with the aid of the GaussView 6.0 software [32]. Our findings were based on the B3LYP, B3PW91 and CAM-B3LYP functional. The 6-311G(d) basis set was used for this purpose. According to Ejuh et al. [33,34] and Tadjouteu Assatse et al. [35], B3LYP is as an efficient and precise functional for the prediction of molecular structures and the determination of the energies. As regards the B3PW91 functional, due to the consideration of gradient corrections, it is one of the most efficient in calculations taking into account energy; it allows an accurate determination of electronics properties with a small mean absolute deviation from the experimental values [36]. Regarding to the CAM-B3LYP functional, it takes into account long-range interactions and should lead to good values of the nonlinear optical parameters.

Simulations began by the geometric optimization of our molecules, followed by determining the stability of the modeled system by calculating the binding energies using the following equations:

$$E_{b,1} = E(fCNT) - E(C_{15}H_{23}O_5) - E(CNTfC_2H_4N) + E_{BSSE,1} \quad (1)$$

$$E_{b,2} = E(2fCNT) - 2E(C_{15}H_{23}O_5) - E(C_2H_4NfCNTfC_2H_4N) + E_{BSSE,2} \quad (2)$$

where $E(fCNT)$ and $E(2fCNT)$ represent the total electronic energies of the functionalized carbon nanotube once and twice, respectively. $E(C_{15}H_{23}O_5)$ is the electronic energy of the dihydroartemisinin radical (DHA − H). $E(CNTfC_2H_4N)$ is the electronic energy of the functionalized carbon nanotube with the azomethine ylide functional group, and $E(C_2H_4NfCNTfC_2H_4N)$ the electronic energy of the carbon nanotube functionalized twice with the azomethine ylide functional group. $E_{BSSE,1}$ and $E_{BSSE,2}$ are the basis set superposition errors (BSSE) energies. They were assessed using the counterpoise method of Boys et al. [37].

Solvation energies of fCNTs and 2fCNTs were assessed by geometrically optimizing our molecular systems in gas phase and in

solvent media using the conductor polarizable continuum model (CPCM) coupled to the universal Solvation Model based on Density (SMD) [38]. The difference between these optimization energies is the Gibbs free energy of solvation.

The linear and nonlinear optical parameters such as dipolar moment (μ), polarizability (α) and anisotropy (Δα), first-order hyperpolarizability (β) of our modeled systems were assessed using equations available in the literature [39]. The molar refractivity (MR), which is a measure of the volume occupied by either a unique atom or a group of atoms, was calculated as follows $MR = \frac{4\pi}{3} N_A \alpha$ [40,41] where N_A is the Avogadro's constant and α the average polarizability [39]. Finally, the HOMO-LUMO energy gap (E_g) was assessed and the global reactivity descriptors were evaluated using the vertical approximation for ionization potential (IP) and electron affinity (EA) [42]. The ionization potential and electron affinity were assessed by the finite difference method [43]. Thus, the fundamental gap, which connecting the ionization potential and the electron affinity is given by [44]

$$E_f = IP - EA \tag{3}$$

The chemical potential

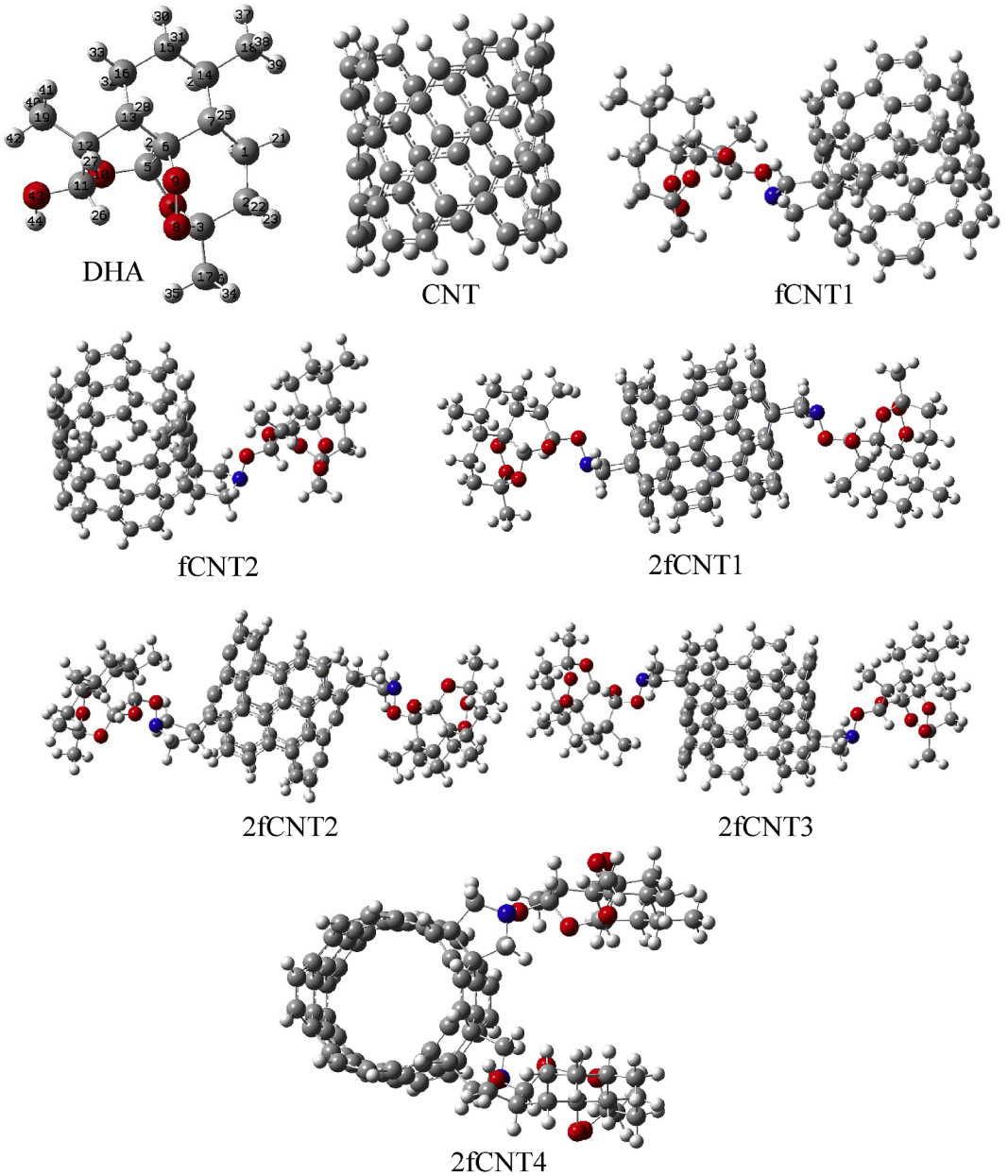

Fig. 1. Optimized structures of studied molecules in gas phase obtained using B3LYP functional. Blue atoms denote nitrogen, reds for oxygen, grays for carbon and whites for hydrogen.

$$\mu_{CP} = -(IP + EA)/2 \tag{4}$$

and the electronegativity $\chi = -\mu_{CP}$, were assessed. The chemical hardness

$$\eta = (IP - EA)/2 \tag{5}$$

the chemical softness [45].

$$S = 1/\eta \tag{6}$$

the electrophilicity index [46].

$$\omega = \mu_{CP}^2/2\eta \tag{7}$$

and the nucleophilicity index

$$\upsilon = 1/\omega \tag{8}$$

were also evaluated. Finally, the electronic charge transfer

$$\Delta N_{max} = -\mu_{CP}/\eta = 2\omega/\chi \tag{9}$$

which is the maximum amount of electronic charge that an electrophile system can accept [43], was assessed. The maximum amount of charge transfer between DHA and functionalized CNTs denoted ECT (electrophilicity-based charge transfer) is given by

$$ECT = (\Delta N_{max})_{fCNTs} - (\Delta N_{max})_{DHA} \tag{10}$$

Thus, if $ECT > 0$, fCNTs acts as electron acceptor and if $ECT < 0$, fCNTs acts as electron donor [47].

3. Results and discussion

3.1. Optimized structures

Fig. 1 shows the graphical representations of the optimized structures of dihydroartemisinin and (5,5) single-wall pristine carbon nanotube (CNT) as well as DHA covalently bound to CNT using 1,3-DC reaction of azomethine ylide. Several functionalization sites were considered and the corresponding nanostructures are denoted fCNT1 and fCNT2 for the first functionalization and, 2fCNT1, 2fCNT2, 2fCNT3, 2fCNT4 for the second functionalization. The optimization was carried out in gas phase and in solvent media. We did not observe a negative frequency after optimization. Some optimized geometry parameters such as bond lengths and bond angles of our investigated molecules, calculated using B3LYP in gas phase, can be found in the supplementary material (S). From Table S1, a significant variation in C–C bond lengths around the functionalization site is observed when moving from virgin CNT to functionalized CNT. As fact, in the pristine CNT the C31–C32 bond length is 1.4248 Å compared to the C31–C32 bond length of 1.6794 Å in the fCNT and to 1.6852 Å in the 2fCNT. Likewise, in the functionalized CNT the C32–C33 bond length is 1.5065 Å compared to the C32–C33 bond length of 1.4392 Å in the pristine CNT. The differences are less than 0.05% as soon as one moves away from the functionalization site. Similar observations can be made on the C–C–C and C–C–H bond angles of the virgin CNT and the functionalized CNT reported in Table S3. According this table, the maximum difference is of the order of 5.58% when moving from the pristine CNT to fCNT and of 5.96% when moving from the pristine CNT to 2fCNT; thus leading to distortions of the carbon nanotube around the functionalization site. As shown in Fig. 1 for 2fCNTs, these local distortions are more localized and increase by approximately 1.72 times when the functionalization takes place on the ends of the carbon nanotube (2fCNT2 case).

The bond lengths of the DHA and the DHA covalently bound to CNT are reported in Table S2. From this table, we observe that the C–C and C–O bond lengths varies slightly when we move from DHA to fCNT. The difference is found between 0.028% and 0.500% for C–O bond and between 0% and 0.065% for C–C bond. This difference is 0.007% for the O–O bond length. We have also recorded in Table S2 the experimental values of the bond lengths of the DHA drug obtained at 103(2) K by Jasinski et al. [48]. Comparing our predicted values with the experimental values, we notice a good agreement with deviations ranging from 0.03% to 2.17%. As regards the DHA bond angles, they are given in Table S4. From this table, one can observe that just like the bond lengths, the value of C–C–C, C–C–H, C–C–O, C–O–O and C–O–H angles varies slightly when moving from DHA to fCNT. The maximum variations obtained are of the order of 1.684% for C–O–H, 1.074% for C–C–H, 0.462% for C–C–C, 0.235% for C–C–O and 0.165% for C–O–O. As for the bond lengths, there is a fairly good agreement between our calculated values of the bond angles and the experimental values [48] with deviations ranging from 0.06% to 6.16%. In view of the above results, it can be concluded that functionalization does not change the molecular structure of DHA.

3.2. Energy analysis and solubility of the modeled systems

The binding energies in gas phase and in water and chloroform media of DHA covalently bound to CNT were assessed using Eqs. (1) and (2) for the first and second functionalization, respectively. The results are collected in Table 1. Binding energy is released when the

DHA drug associates in a targeted way with virgin CNT, thus leading to a lowering of the overall energy of the nanostructure. Lower is the binding energy, more stable is the nanostructure. As shown in Table 1, except for 2fCNT3 and 2fCNT4 configurations which have positive binding energies obtained using B3LYP functional in the gas phase and in solvent media, the binding energies of the other configurations are negative in all three media. This means that the functionalization of DHA on CNT is energetically favorable. According to Table 1, with regard to the first functionalization, the fCNT2 configuration is the most stable whatever the considered media and the calculation method, thus demonstrating a strong interaction between DHA and CNT. In addition, one can see that, in the solvent media, the binding energies are higher in comparison to the gas phase and they are generally lower in chloroform than in water; thus meaning that this drug is more stable in chloroform. Several experimental works were carried out [49-51] to improve the solubility of DHA in water, which is the most suitable solvent for the delivery of this antimalarial drug.

Regarding the 2nd functionalization, it improves the stability by at least 62% when we move from fCNT2 to 2fCNT2 regardless of the considered media and the calculation method. While it is unfavorable when moving from fCNT1 to 2fCNT1 under the same conditions. According to Table 1, the stability of the investigated nanostructures increases when moving from B3LYP to B3PW91 whatever the media. However, the binding energy values of the 2fCNT3 configuration in gas phase decrease by approximately 20.87 times when we move from B3LYP to B3PW91. This is not in agreement with the work carried out by Novikov et al. [52] on the effect of DFT-functional on the calculation of binding energies of carbon [n,5] prismanes. According to the authors, the binding energies obtained for the long [n,5] prismanes with the efficient length of ~150 Å within the B3LYP and B3PW91 functionals can differ by a factor of 1.1. Furthermore, 2fCNT3 is not stable in aqueous solution, therefore this configuration is not suitable for the delivery of two DHA. Finally, the 2fCNT4 configuration is the least stable in the gas phase and the optimization and binding energy calculations in solution did not converged.

The Gibbs free energies of solvation of DHA, CNT and fCNTs are summarized in Table 2. Gibbs' free energy of solvation provides a measure of the solubility of a substance in a solvent. According to Zhou et al. [53], to cross biological barriers, therapeutic molecules should be easily soluble in water. Thus, drugs with the lowest Gibbs free energy of solvation are the most soluble. As can be seen in Table 2, the solvation energies of fCNTs are all negative, thus allowing to conclude from a thermodynamic point of view that the process is spontaneous. Moreover, as the Gibbs free energy of solvation of DHA and fCNTs are less than −12 kcal/mol, these therapeutic molecules can be considered as quality drugs, as predicted by Zafar et al. [54]. In addition, the solvation energies in Table 2 show that the use of fCNTs as nanovectors for drug administration and targeted delivery of therapeutic compounds improves the solubility of this drug and that increasing the functionalization sites also enhances the solubility of the molecule. Finally, just like for the relative stability of the fCNT2 and fCNT1 configurations, the fCNT2 configuration is more soluble than the fCNT1 configuration. The same is true for the 2fCNT2 and 2fCNT1 configurations. Furthermore, compared to fullerene C_{60}, functionalized CNT are more soluble in water than functionalized fullerene [25].

3.3. Electronic properties analysis

The frontier molecular orbitals of the studied molecules are shown in Figs. 2 and 3. They provide qualitative information about the susceptibility of electrons to jump from the HOMO level to the LUMO level. Regions with high electron density are shown in red, while those with low electron density are shown in green. The total electron density maps of DHA, CNT and fCNTs were also evaluated and are shown in Fig. 2 for the DHA drug and the pristine CNT, and in Fig. 3 for the fCNTs. Indeed, molecular electrostatic potential (ESP) map is a suitable method to investigate the charge distribution of the molecular complex. Regions with high electron density are shown in red and yellow, while regions with low electron density are shown in blue. From Fig. 2, we can conclude that oxygen atoms of DHA might be considered as the active site for the interaction with the nitrogen atom belonging to the azomethine ylide functional group. Indeed, the functionalization takes place by establishing a bond between the nitrogen atom belonging to the azomethine ylide functional group and the oxygen atom labeled 43 of the drug DHA.

As shown in Fig. 3, the frontier molecular orbitals of the studied nanostructures are mainly localized on the nanotube. Indeed, the HOMO orbitals are hardly disturbed during the functionalization. While in the case of LUMO, a weak distribution of charges towards the azomethine ylide functional group was observed. However, the functionalization of DHA on CNT through azomethine ylide, still impacts the HOMO-LUMO energy gap of CNT. One important measure of the chemical stability of a molecule is the HOMO-LUMO energy gap; thus, if a molecule has a small or zero HOMO-LUMO gap, it may be chemically reactive [55]. The energy gap (E_g) of the investigated molecules is given in Table 3 for DHA, pristine CNT and for the stable configurations fCNT1-2 and 2fCNT1-2; while the values of E_{HOMO}, E_{LUMO} and E_g of the less stable nanostructures 2fCNT3-4 are summarized in Table S5 of the supplementary material.

Table 1
Binding energy (kcal/mol) for fCNTs in gas phase and in solvent media.

Media	Gas phase		Water		Chloroform	
Nanostructures/Methods	B3LYP	B3PW91	B3LYP	B3PW91	B3LYP	B3PW91
fCNT1	−35.552	−35.811	−32.398	−32.737	−33.106	−33.427
fCNT2	−42.380	−53.644	−33.669	−47.822	−34.256	−49.381
2fCNT1	−9.967	−20.671	−3.246	−13.818	−4.812	−15.419
2fCNT2	−96.083	−98.201	−66.070	−87.129	−55.401	−89.949
2fCNT3	−4.307	−89.900	2.002	−7.301	0.521	−8.819
2fCNT4	2.358	−7.410	–	–	–	–

Table 2
Solvation energy (kcal/mol) for DHA, CNT and fCNTs in water and chloroform media.

Solvent	Water		Chloroform	
Molecules/Methods	B3LYP	B3PW91	B3LYP	B3PW91
DHA	−16.932	−16.896	−7.590	−7.545
CNT	−20.046	−22.072	−12.732	−13.918
fCNT1	−33.624	−35.569	−18.833	−19.942
fCNT2	−34.561	−36.053	−19.186	−20.080
2fCNT1	−47.351	−49.141	−25.023	−26.033
2fCNT2	−48.817	−50.440	−25.505	−26.472
2fCNT3	−49.195	−51.077	−25.496	−26.530

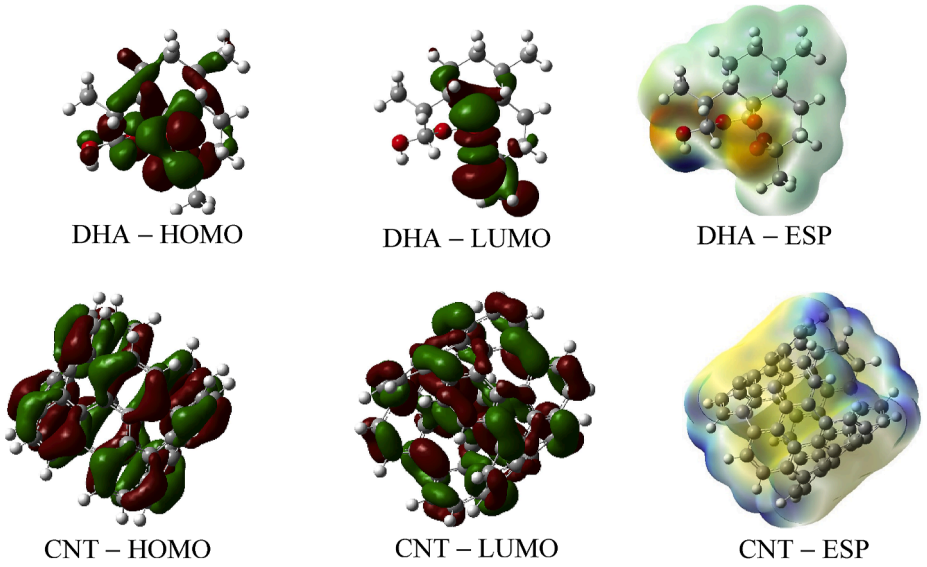

Fig. 2. HOMO-LUMO molecular orbitals and molecular electrostatic potential (ESP) map of DHA and virgin CNT in gas phase obtained using B3PW91 functional.

The electronic sensitivity and the electrical conductivity (σ) of a material are governed by its energy gap through the relation $\sigma \propto \exp(-E_g/2k_BT)$, where k_B is the Boltzmann constant and T the absolute temperature [56]. Therefore, the decrease in E_g leads to an increase of the electrical conductivity, reactivity and sensitivity. The values of E_g in Table 3 show that the functionalization of DHA on CNT improves drug reactivity and sensitivity and CNT conductivity, and the functionalization on several sites further reduces the value of the HOMO-LUMO gap. On the other hand, the value of the energy gap hardly varies when moving from the gas phase to solution. This shows that the conductivity, sensitivity and reactivity of the studied systems hardly changes from gaseous phase into solution. Shakerzadeh et al. [57] in their work have shown that the functional B3PW91 leads to good results of the energy gap. Our findings reveal very slight differences when we move from B3LYP to B3PW91; the results obtained by the two methods can therefore be used indifferently. Thus, the reduction of energy gap in the gas phase is at least 5.8% and 16.9% when moving from virgin CNT to fCNT1 and from virgin CNT to fCNT2, respectively regardless of the calculation method; for the 2nd functionalization, this decrease is at least 5.5% and 16.0% when we move from fCNT1 to 2fCNT1 and from fCNT2 to 2fCNT2, respectively. However, as shown in Table S5 of the supplementary material, the less stable 2fCNT3-4 configurations rather lead to an increase of the E_g. Finally, we can conclude that the two most stable configurations fCNT2 and 2fCNT2 allow the energy gap to go from 1.52 eV for the virgin CNT to 1.27 eV for fCNT2 and to 1.06 eV for 2fCNT2. This last value is comparable to the silicon gap [6] which is an excellent semiconductor. Furthermore, our predicted E_g value of the pristine (5,5) SWCNT agrees with that 1.56 eV reported in the literature [53].

As regards the fundamental gap (E_f), its values are collected in Table 3. In the case of organic molecules, it is important to point out that the fundamental gap generally differs from the HOMO-LUMO electronic gap [44]. In fact, the fundamental gap given by Eq. (3), connects the ionization potential (IP) and the electron affinity (EA) and is also related to the chemical hardness (η) by the relation $E_f = 2\eta$. Therefore, in terms of electronic transition, the fundamental gap is well suited to describe the reactivity of a compound [25]. As can be seen in Table 3, just like for the energy gap, the functionalization of DHA on CNT reduces the fundamental gap which hardly depends on the calculation method. The decrease of E_f in gas phase is at least 5.0% and 9.5% when moving from virgin CNT to fCNT1 and from CNT to fCNT2, respectively. For the functionalization on two sites, this decrease is at least 4.8% and 8.3% when we move from fCNT1 to 2fCNT1 and from fCNT2 to 2fCNT2, respectively. However, unlike E_g, there is a strong decrease of E_f when we move from the gas phase to solvent media. The variation in water is at least 68%, 71%, 69% and 75% for fCNT1-2 and 2fCNT1-2,

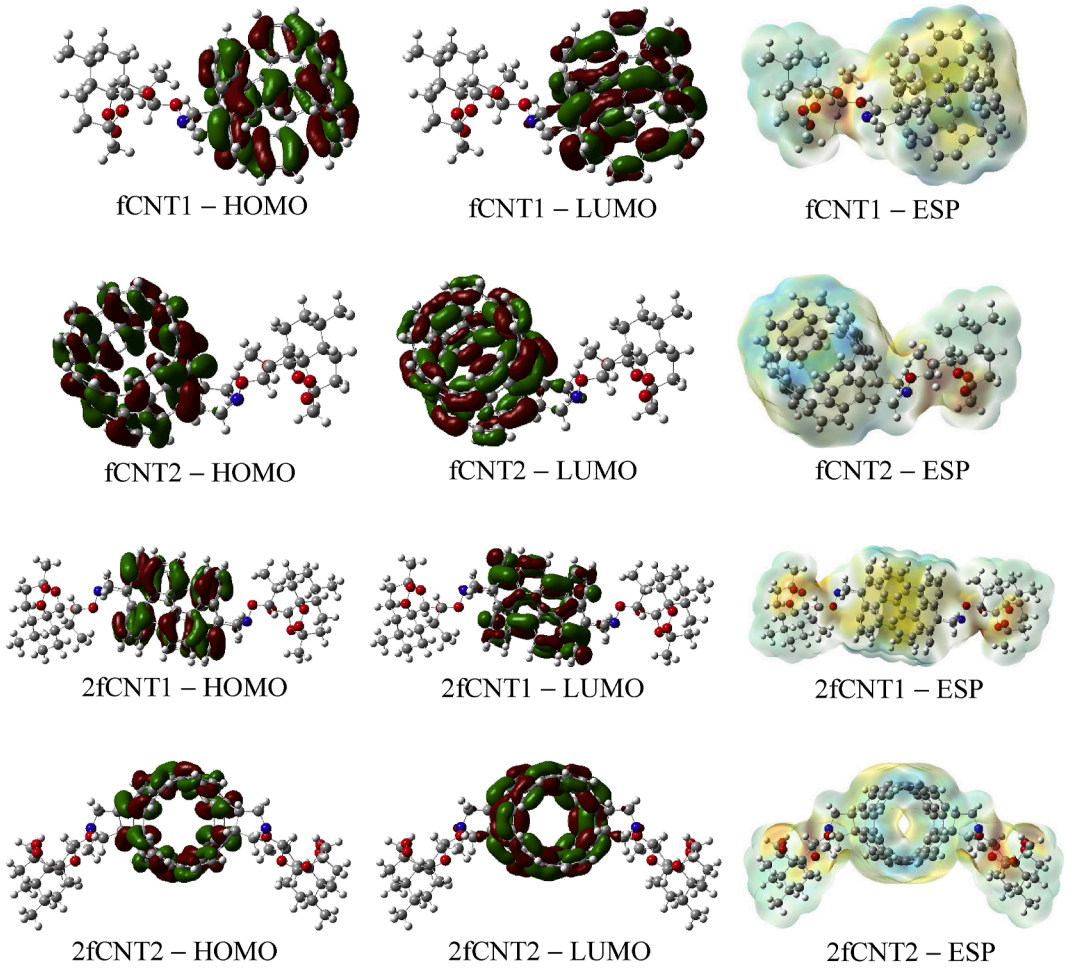

Fig. 3. HOMO-LUMO molecular orbitals and ESP map of our stable therapeutic nanostructures (fCNT1-2 and 2fCNT1-2) in gas phase obtained using B3PW91 functional.

respectively. These decreases in chloroform are at least 54%, 56%, 54% and 59% for fCNT1-2 and 2fCNT1-2, respectively. Similar observations are valid in the case of virgin CNT when moving from gas phase to solution; and to a lesser degree for DHA. Thus, the two most stable configurations fCNT2 and 2fCNT2 allow in the gas phase to reduce the fundamental gap from 3.65 eV for the virgin CNT to 3.30 eV for fCNT2 and to 3.02 eV for 2fCNT2; while in water E_f goes from 1.20 eV for the virgin CNT to 0.95 eV for fCNT2 and to 0.74 eV for 2fCNT2.

3.4. 4- Global reactivity descriptors

The values of the global reactivity descriptors of the studied molecular systems such as ionization potential (IP), electron affinity (EA), chemical potential (μ_{CP}), chemical hardness (η), electrophilicity index (ω), electronic charge transfer ΔN_{max} and electrophilicity-based charge transfer (ECT) obtained using B3LYP and B3PW91 functional in gas phase and in solvent media were assessed using Eqs. (4)-(10) and are summarized in Table 3. The ionization potential is related to the ability to cross the blood-brain barrier [58], while electron affinity is use for the study of optimal bioavailability [59]. The value of IP of the investigated systems increases when we move from gas phase to solution, while the value of EA decreases at the same level, thus leading to a decrease of the fundamental gap when moving from gas phase to solution. However, the values of IP decrease during functionalization while that of EA increases. In addition, the values of IP of DHA are quite high and fall within the range of values given in literature for the majority of drugs, 6 eV $<$ IP $<$ 9 eV [60]; while the EA values are all negative whatever the considered media and fall within the range of values -2 eV and $+3$ eV for most drugs [60].

The chemical hardness gives an account of the resistance of a compound against the modification of its electronic structure and allows to explain the reactivity and the stability of a compound. The higher η is, the more stable and less reactive the compound is. According to the results in Table 3, μ_{CP} and η decrease during the functionalization of DHA on CNT whatever the considered media, thus showing that the stability of DHA decreases while its reactivity increases.

Table 3
Electronic and global reactivity descriptors of DHA [25], CNT and fCNTs in gas phase and in solvent media.

CNT						
Media	Gas phase		Water		Chloroform	
Descriptors/Methods	B3LYP	B3PW91	B3LYP	B3PW91	B3LYP	B3PW91
E_g (eV)	1.524	1.524	1.524	1.523	1.523	1.521
IP (eV)	5.529	5.621	4.444	4.568	4.658	4.772
EA (eV)	1.877	1.971	3.235	3.366	2.946	3.068
E_f (eV)	3.652	3.649	1.209	1.201	1.712	1.704
μ_{CP} (eV)	−3.703	−3.796	−3.840	−3.967	−3.802	−3.920
η (eV)	1.826	1.825	0.605	0.601	0.856	0.852
ω (eV)	3.756	3.948	12.191	13.102	8.443	9.017
ΔN_{max}	2.028	2.080	6.350	6.605	4.442	4.600
E_g (eV)	7.035	7.222	7.015	7.205	7.021	7.211
IP (eV)	8.753	8.725	7.246	7.229	7.552	7.533
EA (eV)	−1.799	−2.001	−0.033	−0.223	−0.423	−0.616
E_f (eV)	10.552	10.726	7.279	7.453	7.975	8.149
μ_{CP} (eV)	−3.477	−3.362	−3.607	−3.503	−3.564	−3.458
η (eV)	5.276	5.363	3.640	3.726	3.988	4.074
ω (eV)	1.146	1.054	1.787	1.647	1.593	1.468
ΔN_{max}	0.659	0.627	0.991	0.940	0.894	0.849
E_g (eV)	1.435	1.426	1.436	1.426	1.436	1.426
IP (eV)	5.266	5.339	4.314	4.424	4.501	4.601
EA (eV)	1.797	1.883	3.194	3.321	2.890	3.006
E_f (eV)	3.469	3.456	1.120	1.102	1.611	1.595
μ_{CP} (eV)	−3.532	−3.611	−3.754	−3.873	−3.695	−3.804
η (eV)	1.734	1.728	0.560	0.551	0.806	0.797
ω (eV)	3.596	3.772	12.588	13.606	8.475	9.071
ΔN_{max}	2.036	2.089	6.706	7.027	4.587	4.770
$ECT_{DHA\text{-}fCNT}$	1.377	1.462	5.715	6.087	3.693	3.921
$ECT_{CNT\text{-}fCNT}$	0.008	0.009	0.356	0.421	0.145	0.169
E_g (eV)	1.267	1.265	1.275	1.273	1.273	1.271
IP (eV)	5.244	5.338	4.275	4.399	4.465	4.581
EA (eV)	1.940	2.036	3.319	3.452	3.017	3.141
E_f (eV)	3.304	3.303	0.956	0.947	1.448	1.440
μ_{CP} (eV)	−3.592	−3.687	−3.797	−3.925	−3.741	−3.861
η (eV)	1.652	1.651	0.478	0.474	0.724	0.720
ω (eV)	3.904	4.116	15.077	16.264	9.666	10.354
ΔN_{max}	2.174	2.233	7.941	8.287	5.168	5.363
$ECT_{DHA\text{-}fCNT}$	1.515	1.606	6.950	7.347	4.274	4.514
$ECT_{CNT\text{-}fCNT}$	0.146	0.152	1.592	1.682	0.726	0.763
E_g (eV)	1.356	1.343	1.353	1.339	1.353	1.340
IP (eV)	5.024	5.082	4.191	4.291	4.352	4.442
EA (eV)	1.723	1.797	3.154	3.276	2.834	2.943
E_f (eV)	3.301	3.286	1.037	1.016	1.518	1.498
μ_{CP} (eV)	−3.373	−3.439	−3.672	−3.784	−3.593	−3.692
η (eV)	1.651	1.643	0.518	0.508	0.759	0.749
ω (eV)	3.447	3.600	13.010	14.094	8.505	9.100
ΔN_{max}	2.044	2.094	7.085	7.450	4.734	4.929
$ECT_{DHA\text{-}fCNT}$	1.385	1.467	6.094	6.510	3.840	4.080
$ECT_{CNT\text{-}fCNT}$	0.015	0.013	0.735	0.844	0.292	0.329
E_g (eV)	1.064	1.058	1.071	1.065	1.069	1.063
IP (eV)	5.027	5.099	4.146	4.258	4.318	4.420
EA (eV)	1.995	2.078	3.392	3.518	3.080	3.195
E_f (eV)	3.032	3.021	0.753	0.740	1.238	1.225
μ_{CP} (eV)	−3.511	−3.589	−3.769	−3.888	−3.699	−3.808
η (eV)	1.516	1.511	0.377	0.370	0.619	0.612
ω (eV)	4.065	4.262	18.858	20.433	11.053	11.836
ΔN_{max}	2.316	2.375	10.007	10.510	5.977	6.217
$ECT_{DHA\text{-}fCNT}$	1.657	1.748	9.016	9.570	5.083	5.368
$ECT_{CNT\text{-}fCNT}$	0.288	0.295	3.657	3.905	1.535	1.617

The electronegativity χ is the negative chemical potential, and there is always a transfer of electron from less electronegative compound to a more electronegative one. The amount of charge transfer between DHA and fCNTs ($ECT_{DHA\text{-}fCNT}$) was assessed based on ΔN_{max}. All $ECT_{DHA\text{-}fCNT}$ values in Table 3 are positive, indicating that the respective fCNTs act as electron acceptors and DHA acts as electron donor; therefore, the charge flows from drug to fCNTs. Likewise, except for 2fCNT3-4, the charge transfer from pristine CNT to fCNTs are all positive, showing that the carbon nanotube behaves as an electron donor (the charge transfer occurs spontaneously from CNT to fCNTs). The values of ω in Table 3 also show that the reactivity of the modeled nanostructures is strongly improved in solvent media and that it is important in water than in chloroform. Therefore, fCNTs are excellent electrophiles in aqueous solution.

In order to better understand the charge transfer between DHA drug and fCNTs, natural bond orbital (NBO) was carried out in gas phase and in water. The increase of the natural atomic charges of the atoms close to the functionalization site when moving from the gas phase into water remains low of the order of 5% for the nitrogen atom and of the order of 1.6% for the oxygen atom involved in the functionalization. We have therefore decided to present the NBO analysis in the aqueous media suitable for DHA drug delivery. The values of natural atomic charges of some atoms close to the functionalization site are summarized in Table 4. Based on the natural atomic charges distribution of DHA alone, the charge of the oxygen atom labeled 43 involved in the functionalization is −0.736 e. This charge reduces to −0.457 e after functionalization. Thus, there was indeed a charge transfer from the drug to the fCNTs. Moreover, as can be seen in Table 4, the natural atomic charges distribution is the same on the two functionalization sites. Finally, from the NBO calculation we found that the distribution of natural atomic charges in the investigated functionalized nanostructures is ranged from −0.629 e to +0.595 e for fCNT1 and 2fCNT1, from −0.629 e to +0.437 e for fCNT2 and 2fCNT2, and for the DHA drug, it is ranged from −0.736 e to +0.595 e.

3.5. 5- Nonlinear optical properties

Some linear and nonlinear optical parameters of our studied systems such as those enumerated in the methodology section were assessed in gas phase using B3LYP, B3PW91 and CAM-B3LYP functional. The values of these parameters are given in Table 5. These properties have been investigated due to their importance in pharmacology [61,62], in biomedical field [63] and in biomedical imaging [64]. According to Ejuh et al. [65] spatial structure and electronic distribution govern interactions between drugs and biological molecules. Thus, the polarity of a molecule comes from the non-homogeneous distribution of its electronic cloud. As regards the polarizability, it measures the ease with which the electronic cloud of a molecule can be deformed under the effect of an electric field or under the effect of another molecule. Therefore, the dipole moment and polarizability provide information about charge distribution within the molecule and thus affect solvation and membrane permeability on the molecule [65]. According to Erol Eroglu and Hasan Trükmen [66], the dipole moment or polarizability is the main factor in inhibition activity, the activity increasing with the dipole moment. In addition, drugs with greater dipole moment are less well absorbed [67]. From Table 5, it is observed that, except for the least stable configuration (2fCNT4), the dipole moments values of the DHA covalently bound to CNT are within the range of values 3 D and 5 D of most drugs given in literature [68]; which implies that our therapeutic nanostructures have high absorption and are actively transported. Further, the dipole moment of all our nanostructures are higher than that of DHA, demonstrating that the functionalization of DHA on CNT improves the polarity of the whole system which is appropriate property for drug delivery in biological systems [69]. Furthermore, since polarizability is a representation of molecular hydrophobicity [70], it is the main factor influencing the binding affinity of the drug [65]. Therefore, the large values of the polarizability of our stable therapeutic nanostructures show that they have excellent binding affinity. As regards the hyperpolarizability, nonlinear optical properties have applications in the second [71,72] and third harmonics generation [63] (SHG and THG), in drug delivery imaging [72-74], in the pharmaceutical and biopharmaceutical field [61,62,64]. NLO imaging is thus a technology with great potential for pharmaceutical analysis. According to several authors [75-77], NLO is more established in the biomedical than pharmaceutical field.

From Table 5, we observed that, except for the first-order hyperpolarizability which varies greatly when moving from B3LYP or B3PW91 to CAM-B3LYP, all the parameters vary slightly with the calculation method, whatever the investigated system. Indeed, unlike the functional B3LYP and B3PW91, the CAM-B3LYP takes into account long-range interactions and should lead to good values of the hyperpolarizability, which explains the strong variations observed.

Regarding the functionalization of DHA on CNT, we found that it strongly improves NLO properties. Indeed, for the first-order hyperpolarizability, the increase is of the order of 432.6%, 519.9% and 98.6% for fCNT1 obtained using B3LYP, B3PW91 and CAM-B3LYP, respectively; and of the order of 737.3%, 943.6% and 291.1% for fCNT2 obtained respectively with the same functionals. Comparing to the virgin nanotube, the first-order hyperpolarizability goes from 0 to higher or lower values depending on the calculation method. Concerning the dipole moment, CNT shows no polarity, however, the dipole moment increases significantly after functionalization due to the change of its electronic density. As regards the polarizability, the increase is at least 400% when moving from DHA to fCNT1,2 whatever the functional, while it is at least 34% when comparing with the virgin nanotube at the same levels. Similar behavior was observed with anisotropy of polarizability. From Table 5, we can also observe that whatever the functional used,

Table 4
The value of natural atomic charges (in e units) of some atoms close to the functionalization site of our stable therapeutic nanostructures in water media obtained using B3PW91 functional.

fCNT1		2fCNT1				fCNT2		2fCNT2			
Atom	Charge	Atom	Charge	Atom	Charge	Atom	Charge	Atom	Charge	Atom	Charge
C31	−0.075	C31	−0.075	C21	−0.074	C1	−0.248	C1	−0.248	C51	−0.244
C32	−0.074	C32	−0.074	C22	−0.075	C2	−0.244	C2	−0.244	C52	−0.248
C81	−0.171	C81	−0.167	C137	−0.233	C87	−0.233	C137	−0.188	C81	−0.188
N82	−0.199	N82	−0.200	C139	−0.168	C89	−0.186	C139	−0.186	N82	−0.211
C83	−0.167	C83	−0.174	C144	0.437	C94	0.437	C144	0.437	C83	−0.186
O97	−0.620	O97	−0.621	O145	−0.447	O95	−0.457	O145	−0.458	O97	−0.622
C98	0.438	C98	0.437	N152	−0.200	N102	−0.211	N152	−0.211	C98	0.437
C99	−0.233	C99	−0.233	O160	−0.619	O110	−0.622	O160	−0.622	C99	−0.233
O107	−0.447	O107	−0.447	C167	−0.170	C117	−0.189	C167	−0.188	O107	−0.458

Table 5
Dipole moment μ (D), average polarizability α_0 ($\times 10^{-24}$ esu), anisotropy of polarizability $\Delta\alpha$ ($\times 10^{-24}$ esu), total value of the first-order hyperpolarizability β_T ($\times 10^{-30}$ esu) and molar refractivity MR (esu.mol^{-1}) of DHA [25], CNT and fCNTs in gas phase.

CNT						DHA				
Methods/Parameters	μ	α_0	$\Delta\alpha$	β_T	MR	μ	α_0	$\Delta\alpha$	β_T	MR
B3LYP	0	96.162	14.450	0	242.608	2.557	25.649	8.152	1.949	64.711
B3PW91	0	95.835	14.260	0	241.783	2.540	25.428	8.035	2.052	64.153
CAM-B3LYP	0	92.387	18.697	0	233.084	2.641	24.876	7.504	1.505	62.760
fCNT1						fCNT2				
B3LYP	4.411	131.445	33.566	10.378	331.625	3.012	131.480	27.875	16.316	331.712
B3PW91	4.686	130.839	33.575	12.722	330.094	3.065	130.751	27.165	21.417	329.873
CAM-B3LYP	4.204	124.026	30.404	2.990	312.907	2.899	124.261	25.225	5.888	313.499
2fCNT1						2fCNT2				
B3LYP	2.443	167.048	69.939	1.051	421.447	3.605	165.827	44.250	4.207	418.366
B3PW91	2.401	166.133	69.953	1.305	419.138	3.645	164.922	44.169	5.449	416.084
CAM-B3LYP	2.824	156.839	58.081	0.025	395.690	3.747	156.733	38.046	0.485	395.424
2fCNT3						2fCNT4				
B3LYP	2.543	170.955	97.601	0.801	431.304	7.138	167.697	40.148	13.287	423.085
B3PW91	2.514	170.034	97.769	1.018	428.980	7.587	166.910	39.887	15.966	421.098
CAM-B3LYP	2.589	161.270	87.217	0.636	406.870	7.071	157.685	37.194	4.261	397.825

fCNT2 gives the best values of NLO parameters than fCNT1 and the anisotropy of polarizability decreases by at least 20% when we move from fCNT1 to fCNT2.

Concerning the second functionalization, Table 5 demonstrates that except for 2fCNT4, the first-order hyperpolarizability decreases in the cases of 2fCNT1-3. This decrease is of the order of 89.9%, 89.7% and 99.2% for B3LYP, B3PW91 and CAM-B3LYP, respectively when moving from fCNT1 to 2fCNT1; around 74.2%, 74.6% and 91.8% when we move from fCNT2 to 2fCNT2 and around 92.3%, 92.0% and 78.7% when moving from fCNT1 to 2fCNT3. However, the first-order hyperpolarizability increases in the order of 28.0%, 25.5% and 42.5% obtained using B3LYP, B3PW91 and CAM-B3LYP, respectively when we move from fCNT1 to 2fCNT4. Regarding the polarizability and regardless of the functional used, the increase is about 26.5%, 26.1%, 30.0% and 27.1% obtained for 2fCNT1, 2fCNT2, 2fCNT3 and 2fCNT4, respectively. For the anisotropy of polarization, the increase is at least 91%, 51%, 187% and 19% obtained at the same levels. Finally, Table 5 shows that the best values of NLO parameters are obtained for 2fCNT2 and 2fCNT4. But as we reported above 2fCNT4 suffers from being less stable.

Regardless of the second or the first functionalization, the large values of NLO parameters of the studied nanostructures are greater than those of urea [78] which is the reference molecule for the NLO properties. As a result, these therapeutic nanostructures may also have excellent NLO applications including SHG and THG [63,71,72].

4. Conclusion

We performed in gas phase and in solution, DFT calculations of DHA covalently bound to (5,5) CNT using 1,3-DC of azomethine ylide in order to assess the role of fCNTs as a nanovector for the targeted delivery of the DHA drug and to predict their electronic and NLO properties.

From our findings of binding energies and Gibbs free energy of solvation, two energetically stable configurations fCNT1-2 in 1st functionalization and four other 2fCNT1-4 in 2nd functionalization including two energetically stable 2fCNT1-2 and two less stable 2fCNT3-4 were identified. Binding energies also revealed that fCTNs are more energetically stable in chloroform than in water. Furthermore, the results of the geometric optimization indicate that the functionalization does not change the molecular structure of DHA. Based on the solvation energies, the use of fCNTs as nanovectors for drug administration and targeted delivery of therapeutic compounds improves the solubility of DHA drug and the increasing of the functionalization sites also improves the solubility of the drug. Furthermore, since solubility is a parameter that significantly influences drug bioavailability, 2nd functionalization contributes more effectively to targeted drug delivery. Finally, the fCNT2 and 2fCNT2 configurations are the most stable and most soluble.

Regarding the HOMO-LUMO gap, we noted that for the most stable configurations, the value of E_g goes from 1.52 eV for virgin CNT to 1.27 eV for the 1st functionalization and to 1.06 eV for the 2nd functionalization regardless of the considered media; thus giving these nanostructures excellent semiconductor properties and promising materials in the manufacture of optoelectronic devices. On the contrary, the fundamental gap varies with the media. Thus, we found that the two most stable configurations allow in the gas phase to reduce the fundamental gap from 3.65 eV for the virgin CNT to 3.30 eV for fCNT2 and to 3.02 eV for 2fCNT2; while in water E_f goes from 1.20 eV for the virgin CNT to 0.95 eV for fCNT2 and to 0.74 eV for 2fCNT2 and in chloroform E_f goes from 1.70 eV for the virgin CNT to 1.44 eV for the 1st functionalization and to 1.23 eV for the 2nd functionalization.

From the chemical hardness values, we found that, during the functionalization of DHA on CNT, the stability of DHA decreases while its reactivity increases whatever the considered media. Based on the values of the electrophilicity index we can also conclude that the reactivity of the modeled nanostructures is strongly improved in aqueous solution.

Based on the high values of the first hyperpolarizability of the investigated nanostructures, greater than those of urea [78], these therapeutic nanostructures are promising materials for NLO applications. Finally, the size of the carbon nanotube certainly has an impact on the results presented here. It would therefore be interesting to investigate the effect of the size of CNT on the properties of the

investigated nanostructures.

Data availability statement

The authors declare that: (i) The datasets generated during and/or analyzed during the current study are available from the corresponding author on reasonable request. (ii) Some data generated or analyzed during this study are included in this published article (and its supplementary information files).

Declaration of competing interest

The authors declare that they have no known competing financial interests or personal relationships that could have appeared to influence the work reported in this paper.

Appendix A. Supplementary data

Supplementary data related to this article can be found at https://doi.org/10.1016/j.heliyon.2022.e12663.

References

[1] S. Iijima, Helical microtubules of graphitic carbon, Nature 354 (1991) 56–58.
[2] X. Wang, K. Vinodgopal, G. Dai, Synthesis of Carbon Nanotubes by Catalytic Chemical Vapor Deposition, IntechOpen, 2019.
[3] L. Scott, Methods for the chemical synthesis of carbon nanotubes: an approach based onhemispherical polyarene templates, Pure Appl. Chem. 89 (6) (2017).
[4] A. Jagadeesan, K. Thangavelu, V. Dhananjeyan, Carbon Nanotubes: Synthesis, Properties and Applications, IntechOpen, 2020.
[5] N. Hynes, R. Sankaranarayanan, M.K.P. Senthamaraikannan, A. Khan, A. Asiri, I. Khan, Synthesis, properties, and characterization of carbon nanotube-reinforced metal matrix composites, Nanocarbon Compos. (2019) 805–830.
[6] C. Kittel, Introduction to Solid State Physics, sixth ed., John Wiley, New York, 1986.
[7] M. Shulaker, G. Pitner, G. Hills, M. Giachino, H. Wong, S. Mitra, High-Performance Carbon Nanotube Field-Effect Transistors, chez IEEE International Electron Devices Meeting, San Francisco, CA, USA, 2014.
[8] P. Hu, J.Z.L. Li, Z. Wang, W. O'Neill, P. Estrela, Carbon nanostructure-based field-effect transistors for label-free chemical/biological sensors, Sensors 10 (2010) 5133–5159.
[9] X. Yao, Y. Zhang, W. Jin, Y. Hu, Y. Cui, Carbon nanotube field-effect transistor-based chemical and biological sensors, Sensors 21 (2021) 995.
[10] A. Martinez, S. Yamashita, Carbon Nanotube-Based Photonic Devices: Applications in Nonlinear Optics, IntechOpen, 2011.
[11] A. Sharma, V. Singh, T. Bougher, B. Cola, A carbon nanotube optical rectenna, Nat. Nanotechnol. 10 (2015) 1027–1032.
[12] S. Kruss, A. Hilmer, J. Zhang, N. Reuel, M.S.B. Mu, Carbon nanotubes as optical biomedical sensors, Adv. Drug Delivery Rev. 65 (115) (2013) 1933–1950.
[13] S. Tatsuura, M. Furuki, Y. Sato, I. Iwasa, M. Tian, H. Mitsu, Semiconductor carbon nanotubes as ultrafast switching materials for optical telecommunications, Adv. Mater. 15 (16) (2003) 534–537.
[14] Z. Liu, J. Robinsonb, S. Tabakmanb, K. Yanga, H. Dai, Carbon materials for drug delivery & cancer therapy, Mater. Today 14 (17–18) (2011) 316–323.
[15] S. Singh, B. Konwar, Carbon nanotube assisted drug delivery of the anti-malarial drug artemesinin and its derivatives: a theoretical nanotechnology approach, J. Bionanosci. 7 (2013) 630–636.
[16] R. Mendes, A. Bachmatiuk, B. Buchner, G. Cunibertib, M. Rummeli, Carbon nanostructures as multi-functional drug delivery, J. Mater. Chem. B 1 (2013) 401–428.
[17] M. Gallo, A. Favila, D. Glossman-Mitnik, DFT studies of functionalized carbon nanotubes and fullerenes as nanovectors for drug delivery of antitubercular compounds, Chem. Phys. Lett. 447 (2007) 105–109.
[18] L. Lacerda, A. Bianco, M. Prato, K. Kostarelos, Carbon nanotubes as nanomedicines: from toxicology to pharmacology, Adv. Drug Delivery Rev. 58 (2006) 1460–1470.
[19] C. Klumpp, K. Kostarelos, M. Prato, A. Bianco, Functionalized carbon nanotubes as emerging nanovectors for the delivery of therapeutics, Biochim. Biophys. Acta 1758 (2006) 404–412.
[20] M. Prato, K. Kostarelos, A. Bianco, Functionalized carbon nanotubes in drug design and discovery, Acc. Chem. Res. 41 (11) (2008) 60–68.
[21] OMS, Rapport 2020 sur le paludisme dans le monde, 2020.
[22] M. Anafcheh, S. Ghanemi, M. Zahedi, Design of new pincer fullerene ligands thorough [2 + 3] cycloaddition of the azomethine ylides to fullerene cage: a DFT study, Mol. Simulat. 46 (17) (2020) 565–572.
[23] S. Novir, M. Aram, Quantum mechanical simulation of Chloroquine drug interaction with C60 fullerene for treatment of COVID-19, Chem. Phys. Lett. 757 (2020), 137869.
[24] B. Aderibigbe, Design of drug delivery systems containing artemisinin and its derivatives, Molecules 22 (12) (2017) 323.
[25] D. Fouejio, R.A.Y. Kamsi, Y.T. Assatse, G.W. Ejuh, J.M.B. Ndjaka, DFT studies of the structural, chemical descriptors and nonlinear optical properties of the drug dihydroartemisinin functionalized on C60 fullerene, Comput. Theor. Chem. 1202 (2021), 113298.
[26] R. Haynes, From artemisinin to new artemisinin antimalarials: biosynthesis, extraction, old and new derivatives, stereochemistry and medicinal chemistry requirements, Med. Chem. 6 (2006) 509–537.
[27] S. Naderi, A. Morsali, M. Bozorgmehr, S. Beyramabadi, Mechanistic, energetic and structural studies of carbon nanotubes functionalised with dihydroartemisinin drug in gas and solution phases, Phys. Chem. Liq. 56 (120) (2017) 1–9.
[28] A. Bianco, K. Kostarelos, C. Partidos, M. Prato, Biomedical applications of functionalised carbon nanotubes, Chem. Commun. 5 (2005) 571–577.
[29] X. Lu, F. Tian, X. Xu, N. Wang, Q. Zhang, A theoretical exploration of the [1,3]-dipolar cycloadditions onto the sidewalls of (n,n) armchair single-wall carbon nanotubes, J. Am. Chem. Soc. 125 (2003) 10459–10464.
[30] V. Georgakilas, K. Kordatos, M. Prato, D. Guldi, M. Holzinger, A. Hirsch, Organic functionalization of carbon, J. Am. Chem. Soc. 124 (15) (2002) 760–761.
[31] M. Frisch, G. Trucks, H. Schlegel, G. Scuseria, M. Robb, J. Cheeseman, G. Scalmani, V. Barone, B. Mennucci, G. Petersson, H. Nakatsuji, M. Caricat, X. Li, H. Hratchian, A. Izmaylov, J. Bloino, G. Zheng, Gaussian 09, Revision D01, Gaussian, Inc., Wallingford CT, 2013.
[32] R. Dennington, J. Keith, J. Millam, Gauss View, Version 6, Semichem Inc, Shawnee Mission, 2016.
[33] G.W. Ejuh, F.T. Nya, M.T.O. Abe, F.F. Jean-Baptiste, J.M.B. Ndjaka, Electronic structure, physico-chemical, linear and non linear optical properties analysis of coronene, 6B-, 6N-, 3B3N-substituted C24H12 using RHF, B3LYP and wB97XD methods, Opt. Quant. Electron. 49 (111) (2017) 382.
[34] G.W. Ejuh, S. Nouemo, F.T. Nya, J.M.B. Ndjaka, Computational determination of the electronic and nonlinear optical properties of the molecules 2-(4-aminophenyl) quinoline, 4-(4-aminophenyl) quinoline, anthracene, anthraquinone and phenanthrene, Matter. Lett. 178 (2016) 221–226.

[35] Y.T. Assatse, G.W. Ejuh, R.A.Y. Kamsi, F. Tchoffo, J.M.B. Ndjaka, Theoretical studies of nanostructures modeled by the binding of Uracil derivatives to functionalized (5,5) carbon nanotubes, Chem. Phys. Lett. 731 (2019), 136602.
[36] A.D. Becke, Density-functional thermochemistry. III. The role of exact exchange, J. Chem. Phys. 98 (17) (1993) 5648–5652.
[37] S. Boys, F. Bernardi, The calculation of small molecular interactions by the differences of separate total energies. Some procedures with reduced errors, Mol. Phys. 19 (14) (1970) 553–566.
[38] A. Marenich, C. Cramer, D. Truhlar, Universal solvation model based on solute electron density and on a continuum model of the solvent defined by the bulk dielectric constant and atomic surface tensions, J. Phys. Chem. B 113 (2009) 6378–6396.
[39] R.Y. Kamsi, G. Ejuh, P. Mkounga, J. Ndjaka, Study of the molecular structure, electronic and chemical properties of Rubescin D molecule, Chin. J. Phys. 63 (2020) 104–121.
[40] R. Sawale, T. Kalyankar, R. George, S. Deosarkar, Molar refraction and polarizability of antiemetic drug 4-amino-5-chloro-N-(2-(diethylamino)ethyl)-2 methoxybenzamide hydrochloride monohydrate in {Aqueous-Sodium or lithium chloride} solutions at 30 °C, J. Appl. Pharmaceut. Sci. 6 (103) (2016) 120–124.
[41] J. Padrón, R. Carrasco, R. Pellón, Molecular descriptor based on a molar refractivity partition using Randictype graph-theoretical invariant, J. Pharm. Pharmaceut. Sci. 5 (13) (2002) 267–274.
[42] R. Parr, R. Pearson, Absolute hardness: companion parameter to absolute electronegativity, J. Am. Chem. Soc. 105 (1983) 7512–7516.
[43] R.A.Y. Kamsi, G.W. Ejuh, Y.T. Assatse, C.A. Njeumen, F. Tchoffo, J.M.B. Ndjaka, Computational study of reactivity and solubility of Rubescin D and E molecules in gas phase and in solvent media using Hartree-Fock and DFT methods, Chin. J. Phys. 60 (2019) 1–11.
[44] J.-L. Bredas, Mind the Gap 1, Royal Society of Chemistry (Materials Horzons), 2014, pp. 17–19.
[45] W. Yang, R.G. Parr, Hardness, softness, and the fukui function in the electronic theory of metals and catalysis, Proc. Natl. Acad. Sci. U. S. A. 82 (1985) 6723–6726.
[46] R.G. Parr, L.V. Szentpály, S. Liu, Electrophilicity index, J. Am. Chem. Soc. 121 (19) (1999) 1922–1924.
[47] J. Padmanabhan, R. Parthasarathi, V. Subramanian, P.K. Chattaraj, Electrophilicity-based charge transfer descriptor, J. Phys. Chem. A 111 (2007) 1358–1361.
[48] J.P. Jasinski, R.J. Butcher, H.S. Yathirajan, B. Narayanad, T.V. Sreevidya, Redetermination of dihydroartemisinin at 103 (2) K, Acta Cryst. E Struct. Rep. Online 64 (11) (2008) o89–o90.
[49] M.T. Ansari, I. Iqbal, V.B. Sunderland, Dihydroartemisinin-cyclodextrin complexation: solubility and stability, Arch Pharm. Res. 32 (11) (2009) 155–165.
[50] M.T. Ansari, K.T. Batty, I. Iqbal, V.B. Sunderland, Improving the solubility and bioavailability of dihydroartemisinin by solid dispersions and inclusion complexes, Arch Pharm. Res. 34 (15) (2011) 757–765.
[51] M.T. Ansari, I. Ahmad, S.S.U. Hassan, I. Tariq, G. Murtaza, Solubility enhancement of dihydroartemisinin using mixture of hydroxypropyl-β-cyclodextrin and PEG-6000, Lat. Am. J. Pharm. 33 (13) (2014) 483–491.
[52] N.V. Novikov, M.M. Maslov, K.P. Katin, V.S. Prudkovskiy, Effect of DFT-functional on the energy and electronic characteristics of carbon compounds with the unconventional geometry of the framework, Lett. Mater. 7 (14) (2017) 433–436.
[53] Z. Zhou, M. Steigerwald, M. Hybertsen, L. Brus, R.A. Friesner, Electronic structure of tubular aromatic molecules derived from the metallic (5,5) armchair single wall carbon nanotube, J. Am. Chem. Soc. 126 (2004) 3597–3607.
[54] A. Zafar, J. Reynisson, Hydration free energy as a molecular descriptor in drug design: a feasibility study, Mol. Inf. 35 (2016) 207–214.
[55] H.S. Sayiner, F. Kandemirli, S.S. Dalgic, M. Monajjemi, F. Mollaamin, Carbazochrome carbon nanotube as drug delivery nanocarrier for antibleeding drug: quantum Chemical Study, J. Mol. Model. 28 (111) (2022).
[56] A.K. Srivastava, S.K. Pandey, N. Misra, A computational study on semiconducting Si60, Si59Al and Si59P, Chem. Phys. Lett. 691 (2018) 82–86.
[57] E. Shakerzadeh, F. Kazemimoghadam, E.C. Anota, How does lithiation affect electro-optical features of corannulene (C20H10) and quadrannulene (C16H8) buckybowls, J. Electron. Mater. 47 (2018) 2348–2358.
[58] M.C. Hutter, Prediction of blood–brain barrier permeation using quantum chemically derived information, J. Comput. Aided Mol. Des. 17 (17) (2003) 415–433.
[59] J.V. Turner, D.J. Maddalena, S. Agatonovic-Kustrin, Bioavailability prediction based on molecular structure for a diverse series of drugs, Pharmaceut. Res. 21 (11) (2004) 68–82.
[60] A.M. Matuszek, J. Reynisson, Defining known drug space using DFT, Mol. Inf. 35 (12) (2016) 46–53.
[61] A.L. Fussell, A. Isomäki, C.J. Strachan, Nonlinear optical imaging – introduction and pharmaceutical applications, Am. Pharmaceut. Rev. 16 (6) (2013) 54–63.
[62] A.M. Sherman, N. Takanti, J. Rong, G.J. Simpson, Nonlinear optical characterization of pharmaceutical formulations, Trends Anal. Chem. 140 (2021) 1116241.
[63] B. Gu, C. Zhao, A. Baev, K. Yong, S. Wen, P.N. Prasad, Molecular nonlinear optics: recent advances and applications, Adv. Opt. Photon 8 (12) (2016) 328–369.
[64] A.S.M. Waliullah, Recent advances and applications of nonlinear optical microscopy: perspectives in cancer imaging, OSF Preprints (2018).
[65] G. Ejuh, C. Fonkem, Y.T. Assatse, R.Y. Kamsi, T. Nya, L. Ndukum, J. Ndjaka, Study of the structural, chemical descriptors and optoelectronic properties of the drugs Hydroxychloroquine and Azithromycin, Heliyon 6 (18) (2020).
[66] E. Eroglu, H. Turkmen, A DFT-based quantum theoretic QSAR study of aromatic and heterocyclic sulfonamides as carbonic anhydrase inhibitors against isozyme, CA-II, J. Mol. Graph. Model. 26 (2007) 701–708.
[67] S. Agatonovic-Kustrin, R. Beresford, A. Yusof, Theoretically-derived molecular descriptors important in human intestinal absorption, J. Pharmaceut. Biomed. Anal. 25 (2001) 227–237.
[68] A. Matuszek, Defining Known Drug Space by DFT Based Molecular Descriptors. Virtual Screening for Novel Atg5-Atg16 Complex Inhibitors for Autophagy Modulation, Ph.D Thesis, 2014.
[69] Z. Shariatinia, S. Shahidi, A DFT study on the physical adsorption of cyclophosphamide derivatives on the surface of fullerene C60 nanocage, J. Mol. Graph. Model. 52 (2014) 71–81.
[70] C. Gu, X. Jiang, X. Ju, G. Yu, Y. Bian, QSARs for the toxicity of polychlorinated dibenzofurans through DFT-calculated descriptors of polarizabilities, hyperpolarizabilities and hyper-order electric moments, Chemosphere 67 (2007) 1325–1334.
[71] D. Wanapun, U.S. Kestur, D.J. Kissick, G.J. Simpson, L.S. Taylor, Selective detection and quantitation of organic molecule crystallization by second harmonic generation microscopy, Anal. Chem. 82 (113) (2010) 5425–5432.
[72] U.S. Kestur, D. Wanapun, S.J. Toth, L.A. Wegiel, G.J. Simpson, L.S. Taylor, Nonlinear optical imaging for sensitive detection of crystals in bulk amorphous powders, J. Pharmaceut. Sci. 101 (111) (2012) 4201–4213.
[73] C.J. Strachan, M. Windbergs, H.L. Offerhaus, Pharmaceutical applications of non-linear imaging, Int. J. Pharm. 417 (2011) 163–172.
[74] R. Mouras, G. Rischitor, A. Downes, D. Salter, A. Elfick, Nonlinear opticalmicroscopy for drug delivery monitoring and cancer tissue imaging, J. Raman Spectrosc. 41 (18) (2010) 848–852.
[75] C. Krafft, B. Dietzek, J. Popp, Raman and CARS microspectroscopy of cells and tissues, Analyst 134 (16) (2009) 1046–1057.
[76] J.P. Pezacki, J.A. Blake, D.C. Danielson, D.C. Kennedy, R.K. Lyn, R. Singaravelu, Chemical contrast for imaging living systems: molecular vibrations drive CARS microscopy, Nat. Chem. Biol. 7 (13) (2011) 137–145.
[77] R. Mouras, P. Bagnaninchi, A. Downes, A. Elfick, Multimodal, label-free nonlinear optical imaging for applications in biology and biomedical science, J. Raman Spectrosc. 44 (2013) 1373–1378.
[78] C. Cassidy, J.M. Halbout, W. Donaldson, C.L. Tang, Nonlinear optical properties of urea, Opt. Commun. 29 (12) (1979).